

Multiport Frequency-Dependent Network Equivalencing Based on Simulated Time-Domain Responses

Andrea Ubolli, *Member, IEEE*, and Bjørn Gustavsen, *Senior Member, IEEE*

Abstract—This paper presents a multiport implementation of the time-domain-vector-fitting algorithm (TD-VF) for achieving a common-pole rational model approximation from simulated time-domain responses. Similar to the frequency-domain counterpart of the algorithm, a fast realization of TD-VF is achieved based on QR-factorization with consideration of sparsity. The computational speed is further increased by an adaptive downsampling procedure which removes rows from the system matrices. The required model order is reduced by low-pass filtering the input responses, giving a model that is essentially free of spurious Gibbs-like oscillations. The resulting model is directly compatible with Electromagnetic Transients Program-type simulation programs. The multiport TD-VF is applied for the calculation of a frequency-dependent network equivalent (FDNE) of two subnetworks: a 24-kV distribution system and a 145-kV regional transmission system. We show that the procedure offers advantages by achieving faster simulations and reduced memory requirements. In addition, the procedure often enables the use of a shorter time-step length than with the detailed subnetwork representation, thereby achieving further reductions in computational time.

Index Terms—Digital filtering, finite impulse response (FIR), frequency-dependent network equivalent (FDNE), macromodel, multiport formulation, QR factorization, rational approximation, time-domain vector fitting.

I. INTRODUCTION

THE simulation of electromagnetic transients in electric power systems [1] often requires modeling large portions of the system in detail. This is typically the case when studying switching and fault transients as the relatively low-frequency content permits the transients to penetrate very far in the system during the event. At the same time, the need for capturing the high-frequency contents of the waveform may dictate the use of a small simulation time-step length. The combination of a small time step and a large system model often places tough requirements on the computer resources in terms of central-processing

unit (CPU) time and memory requirements, in particular, if the system includes many overhead lines and underground cables.

One way of reducing the computational burden is by replacing parts of the system with a computationally efficient model. These models can be formulated as frequency-dependent black-box terminal equivalents based on rational functions, also known as frequency-dependent network equivalents (FDNEs) [2]–[10]. These models can be easily interfaced with Electromagnetic Transients Program (EMTP)-type simulation platforms via a lumped circuit equivalent [2], [3] or by recursive convolution [11], [12].

FDNEs have traditionally been established in the frequency domain using an admittance formulation. Curve-fitting techniques based on weighted polynomials [13], [14] or pole relocation (vector fitting) [15] are applied for fitting the rational model to the admittance over a given frequency band. The extracted model is subjected to perturbation [16], [17] in order to ensure passivity of the model and, thus, stable simulation.

With some EMTP-type circuit simulators, the calculation of the admittance frequency-domain data is not straightforward and so it becomes a natural choice to base the FDNE identification on simulated time-domain responses. This has traditionally been achieved by means of the ARMA model [5]. It has, however, been shown [18] that the time-domain counterpart of vector fitting (TD-VF) [19] offers several advantages over ARMA by being more robust and accurate, and because stable poles can be guaranteed.

In this paper, we show a practical procedure for adopting TD-VF to FDNE modeling and simulation. A filtering approach is first applied to the input data (time-domain responses) to reduce the required model order and for avoiding spurious high-frequency oscillations in the model's responses. A highly efficient (sparse) multiport formulation of TD-VF is implemented for calculating a rational model with common poles, including a thresholding approach for reducing the number of rows in the system matrices. The modeling procedure is demonstrated for two application examples: 1) a distribution system and 2) a regional transmission system. The inclusion of embedded sources in the model is also shown.

II. PRELIMINARIES

A. Frequency-Dependent Network Equivalent (FDNE)

The objective is to represent parts (subnetworks) of a complex power system with a low-order model with respect to a set of terminals. We define input variables $\{\lambda_i(t)\}$ (voltages

Manuscript received January 24, 2011; revised June 02, 2011; accepted September 28, 2011. Date of current version March 28, 2012. This work was supported by the KMB project "Electric power systems for subsea processing and transportation of oil and gas," financed by the Norwegian Research Council Petromaks programme and industry partners. Paper no. TPWRD-00067-2011.

A. Ubolli is with the Department of Electric Power Engineering, Norwegian University of Science and Technology, Trondheim N-7491, Norway (e-mail: andrea.ubolli@elkraft.ntnu.no).

B. Gustavsen is with SINTEF Energy Research, Trondheim N-7465, Norway (e-mail: bjorn.gustavsen@sintef.no).

Color versions of one or more of the figures in this paper are available online at <http://ieeexplore.ieee.org>.

Digital Object Identifier 10.1109/TPWRD.2011.2173769

or currents) and output variables $\{\psi_j(t)\}$ (currents or voltages) with $i, j = 1 \dots P$ being P the number of ports. In this paper, we shall assume that the subnetwork is a linear time-invariant system (LTI).

The subnetwork is to be replaced with an equivalent mathematical representation that should reproduce as closely as possible the terminal behavior of the original network. Mathematically, the relation between inputs and outputs of this FDNE can be expressed in the time domain as a convolution

$$\psi_{ij}(t) = \int_{-\infty}^{+\infty} h_{ij}(t - \tau) \lambda_j(\tau) d\tau \quad (1)$$

where $\lambda_j(t)$ is the excitation at the j th terminal, $\psi_{ij}(t)$ is the output response at the i th terminal due to excitation $\lambda_j(t)$, and $h_{ij}(t)$ is the impulse response of the element (i, j) .

Analogously, (1) can be brought in the frequency domain by (2), being $s = \sigma + j\omega$ the Laplace variable and H_{ij} being the transfer function impulse response

$$\Psi_{ij}(s) = H_{ij}(s) \Lambda_j(s). \quad (2)$$

B. FDNE Representation by Rational Function

The FDNE will be represented by the multiport rational function (3) with common poles $\{p_n\}$ and order N . The modeling process amounts to identifying the poles $\{p_n\}$ and residue matrices $\{\mathbf{R}_n\}$.

$$\mathbf{H}(s) \cong \sum_{n=1}^N \frac{\mathbf{R}_n}{s - p_n} + \mathbf{R}_0. \quad (3)$$

In this paper, we will assume an admittance formulation $\mathbf{H} = \mathbf{Y}$ (4) that relates voltage excitations to current responses

$$\mathbf{i}(s) = \mathbf{Y}(s)\mathbf{v}(s). \quad (4)$$

C. Extraction of FDNE From Time-Domain Data

The identification of (3) in this paper is performed in the time domain (1) with the data (input and output responses) computed using a circuit simulator. An excitation $\lambda_j(t)$ (voltage) is applied to the external terminals, $j = 1 \dots P$, while observing the output responses $\psi_{ij}(t)$ (current) at the same terminals. In this manner, a $P \times P$ matrix of responses $\boldsymbol{\psi}(t)$ is obtained as well as a $P \times P$ matrix $\boldsymbol{\lambda}(t)$ of excitations since, in practice, these excitations could be different for each output response.

The data are used as input for the TD-VF algorithm [19], allowing to identify the poles and residues of the rational function (3) and, hence, the determination of the FDNE.

D. Embedded Sources

The FDNE procedure can also cover situations with stationary sinusoidal sources embedded in the subnetwork. This way, the presence of generators can, as a first approximation, be taken into account. For instance, by representing synchronous

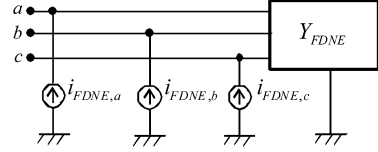


Fig. 1. Current sources i_{FDNE} for the Norton equivalent.

generators by a fixed voltage source at fixed frequency (ω_0) behind an impedance (Thevenin equivalent), a Norton-type FDNE equivalent can be established as follows.

- 1) The current responses with respect to the external terminals are obtained with the (embedded) voltage sources shorted. These responses are used for obtaining the rational model (3) via TD-VF and, hence, the admittance \mathbf{Y}_{FDNE} of the FDNE.
- 2) Using the circuit simulator and the detailed subnetwork representation, the open-circuit terminal voltages \mathbf{v}_0 are obtained with the embedded sources active.
- 3) In the FDNE model, the embedded sources are represented by current sources \mathbf{i}_{FDNE} from ground to the external terminals, see Fig. 1. These sources are obtained by

$$\mathbf{i}_{\text{FDNE}}(\omega_0) = \mathbf{Y}_{\text{FDNE}}(\omega_0)\mathbf{v}_0(\omega_0). \quad (5)$$

E. Interfacing FDNE With the Circuit Simulator

The admittance representation (3) can be interfaced with EMTP-type programs using a lumped circuit representation [2] or by convolution [11] via a companion model (Norton equivalent). In this paper, we make use of the convolution approach as implemented in the PSCAD/EMTDC circuit simulator by a user-defined component [12].

III. TIME-DOMAIN VECTOR FITTING

A. Scalar Formulation

We consider a scalar LTI system in which the excitation $u(t_k)$ and output response $y(t_k)$ are given, with $k = 1 \dots K$ being the time-domain samples. The objective is to identify poles $\{p_n\}$ and residues $\{r_n\}$ of the rational function (3).

The original formulation of the VF algorithm in the frequency domain [15] enables writing the relation (6) between input (U) and output (Y), where $\sigma(s)$ is the weight function, N is the order, $\{\theta_n\}$ and $\{m_n\}$ are unknowns, and $\{q_n\}$ are a set of initial poles

$$\overbrace{\left(1 + \sum_{n=1}^N \frac{\theta_n}{s - q_n}\right)}^{\sigma(s)} Y(s) = \left(\sum_{n=1}^N \frac{m_n}{s - q_n} + m_0\right) U(s). \quad (6)$$

Applying the inverse Laplace transform to each term of (6) and successively discretizing the obtained convolution integral

and simplifying notation [19], [18] gives the time-domain relation (7) where terms $\tilde{u}_n(t)$ and $\tilde{y}_n(t)$ are dependent on the numerical integration method employed in the discretization

$$y(t) = \sum_{n=1}^N m_n \tilde{u}_n(t) - \sum_{n=1}^N \theta_n \tilde{y}_n(t) + m_0 u(t). \quad (7)$$

Expression (7) is written for each input dataset point $t_k = k\Delta t$ in the time domain, with Δt being the time-step length. The resulting overdetermined linear system is solved in the least-squares (LS) sense and an improved poles set $\{q_n\}$ is computed from the solution (7) [18], [19]. Only the set $\{\theta_n\}$ of the unknowns is used for computing the new set of poles $\{q_n\}$. This pole relocating procedure usually converges in a few iterations to the final pole set of the rational function (3), $\{q_n\} \rightarrow \{p_n\}$.

The residues $\{r_n\}$ are finally computed by solving another linear LS system

$$y(t) = \sum_{n=1}^N r_n \tilde{u}_n(t) + r_0 u(t). \quad (8)$$

B. Numerical Integration

The TD-VF expression (7) results from time-domain discretization of the continuous relation (6). Here, $\tilde{u}_n(t)$ and $\tilde{y}_n(t)$ are expressed recursively according to the adopted numerical integration scheme. With trapezoidal integration, the expression becomes (9) [18]. (We only show $\tilde{u}_n(t)$ since $\tilde{y}_n(t)$ has the same form.)

$$\tilde{u}_n(t_k) = \frac{2 + q_n \Delta t}{2 - q_n \Delta t} \tilde{u}_n(t_{k-1}) + \frac{\Delta t}{2 - q_n \Delta t} [u(t_k) + u(t_{k-1})]. \quad (9)$$

C. Multiport Formulation

In the multiport case, the matrix of output responses $\{\psi_{ij}(t)\}$ is stacked into a column $\{y^{(\nu)}(t)\}$, $\nu = 1 \dots L$, with $\nu = i + (j - 1)P$ and $L = P^2$ being the number of responses. Similarly, the set of excitations is stacked into a column of responses $\{u^{(\nu)}(t)\}$. Equation (7) is applied to each pair $\{u^{(\nu)}(t), y^{(\nu)}(t)\}$, giving the sparse linear system (10), see Appendix A. All unknowns $\{m_n^{(\nu)}\}$ and $\{\theta_n\}$ of (7) are collected into arrays $\mathbf{m}^{(\nu)}$ and $\boldsymbol{\theta}$, respectively. In order to have a common set of poles in the rational function (3), the array $\boldsymbol{\theta}$ is the same for all responses

$$\begin{pmatrix} \tilde{\mathbf{U}}^{(1)} & & & \tilde{\mathbf{Y}}^{(1)} \\ & \tilde{\mathbf{U}}^{(2)} & & \tilde{\mathbf{Y}}^{(2)} \\ & & \ddots & \vdots \\ & & & \tilde{\mathbf{U}}^{(L)} & \tilde{\mathbf{Y}}^{(L)} \end{pmatrix} \begin{pmatrix} \mathbf{m}^{(1)} \\ \vdots \\ \mathbf{m}^{(L)} \\ \boldsymbol{\theta} \end{pmatrix} = \begin{pmatrix} \mathbf{y}^{(1)} \\ \vdots \\ \mathbf{y}^{(L)} \end{pmatrix}. \quad (10)$$

All blocks $\tilde{\mathbf{U}}^{(\nu)}$ and $\tilde{\mathbf{Y}}^{(\nu)}$ in (10) are matrices (associated with the ν th pair of responses) of which the k th line is formed by the row array $[\tilde{u}_1^{(\nu)}(t_k) \dots \tilde{u}_N^{(\nu)}(t_k) u^{(\nu)}(t_k)]$ and $[\tilde{y}_1^{(\nu)}(t_k) \dots \tilde{y}_N^{(\nu)}(t_k)]$, respectively.

Finally, the residues are calculated by independently solving (8) for all pairs of responses.

D. Sparse Implementation

The system (10) is solved for the only useful unknown $\boldsymbol{\theta}$ by taking advantage of its sparsity [20], [21]. A factorization QR of each block $\mathbf{G}^{(\nu)}$ (11) is first computed (12)

$$\mathbf{G}^{(\nu)} = \begin{bmatrix} \tilde{\mathbf{U}}^{(\nu)} & \tilde{\mathbf{Y}}^{(\nu)} \end{bmatrix} \quad (11)$$

$$\mathbf{G}^{(\nu)} = \mathbf{G}_Q^{(\nu)} \mathbf{G}_R^{(\nu)}. \quad (12)$$

From each factorization (12), the last N columns of $\mathbf{G}_Q^{(\nu)}$ and the $N \times N$ right bottom square block of $\mathbf{G}_R^{(\nu)}$ are used for building a new system matrix \mathbf{A}_s and corresponding right-hand side \mathbf{b}_s (13). We refer to [20] and [21] for further details. This new system is solved with respect to the unknown $\boldsymbol{\theta}$ (which is used for computing the new poles)

$$\mathbf{A}_s = \begin{pmatrix} \mathbf{G}_R^{(1)} \\ \vdots \\ \mathbf{G}_R^{(L)} \end{pmatrix}, \quad \mathbf{b}_s = \begin{pmatrix} (\mathbf{G}_Q^{(1)})^T \mathbf{y}^{(1)} \\ \vdots \\ (\mathbf{G}_Q^{(L)})^T \mathbf{y}^{(L)} \end{pmatrix}. \quad (13)$$

The solution of (13) requires much less CPU time than that of (10) since the dimension of the system matrix \mathbf{A}_s has been reduced, from $KL \times (N + NL + L)$ to $NL \times N$, assuming a constant number of samples K for each time series, with K generally being much greater than N . Column scaling is applied for solving (13), similarly as in [22].

E. Adaptive Sampling

The number of rows in each $\mathbf{G}^{(\nu)}$ (11) is directly proportional to the number of samples in the time series. In order to expedite the QR factorization (12) and the subsequent solving (13), we remove rows from $\mathbf{G}^{(\nu)}$ while retaining their essential information. (Note, however, that all samples are required to build each $\mathbf{G}^{(\nu)}$ from $\tilde{\mathbf{U}}^{(\nu)}$ and $\tilde{\mathbf{Y}}^{(\nu)}$ (11) according to (9), before the deletion process can be started).

The removal of rows from $\mathbf{G}^{(\nu)}$ is based on a simple ‘‘adaptive sampling’’ rule applied to the original ν th response $y^{(\nu)}(t)$. With a given relative threshold δ , all rows of the matrix $\mathbf{G}^{(\nu)}$ associated with the samples $y^{(\nu)}(t_k)$ are removed that satisfy the condition (14). This equation defines that a sample $y^{(\nu)}(t_k)$ is redundant if it differs from the linear interpolation value between samples $y^{(\nu)}(t_{k-1})$ and $y^{(\nu)}(t_{k+1})$ by less than a pre-defined value. The condition (14) is applied sequentially over all samples in several iterations before reaching the final result. Typically, 5–10 iterations are used in this paper

$$\left| \frac{y^{(\nu)}(t_{k-1}) + y^{(\nu)}(t_{k+1})}{2} - y^{(\nu)}(t_k) \right| < \delta \max_k \{y^{(\nu)}(t_k)\}. \quad (14)$$

We remark that condition (14) is used when all samples are equidistant in time (first iteration). Subsequent iterations

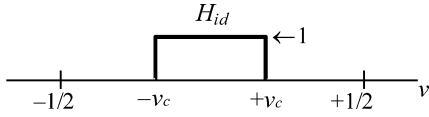
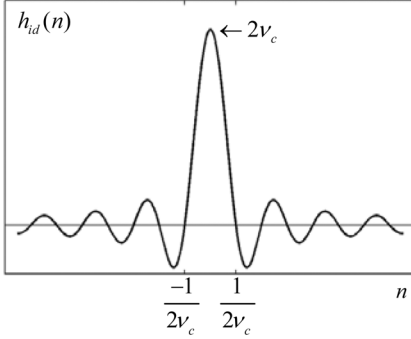


Fig. 2. Ideal low-pass filter in the normalized digital frequency domain.


 Fig. 3. Impulse response h_{id} of an ideal low-pass filter.

use a modified version of (14) which takes into account the nonequidistant sampling.

IV. DIGITAL FILTERING

The dataset of responses $\{y^{(\nu)}(t)\}$ is often characterized by very fast variations and a general nonsmooth behavior. The fast variations are typically associated with wavefronts in systems containing overhead lines and cables. These responses can be very difficult to fit as they generally require very high fitting orders. In order to reduce the high-frequency content and, thus, the required model order, we preprocess the original responses by a low-pass digital filter.

A. Ideal Filter

The ideal low-pass filter can be characterized in the “digital” frequency domain by the transfer function H_{id} (Fig. 2) and in the discrete time domain (Fig. 3) by the impulse h_{id} sequence (15), where n is an integer. The parameter ν ($-0.5 \leq \nu \leq +0.5$) defines the digital frequency (which has been normalized with respect to the sampling frequency $f = (1/\Delta t)$) while ν_c defines the filter cutoff frequency

$$h_{id}(n) = 2\nu_c \text{sinc}(2\nu_c n) = \begin{cases} \frac{1}{\pi n} \sin(2\pi\nu_c n), & n \neq 0 \\ 2\nu_c, & n = 0 \end{cases}. \quad (15)$$

B. Digital FIR Filtering

The ideal low-pass filter is not realizable as a digital filter since its impulse response (15) has infinite time duration. This problem can be alleviated by applying an approximation by a filter response of finite duration, so-called finite impulse response (FIR) filters [23].

C. Practical Implementation

We use the truncated and translated M th-order impulse response h_{FIR} (16) with $(M + 1)$ coefficients, $n = 0 \dots M$, and

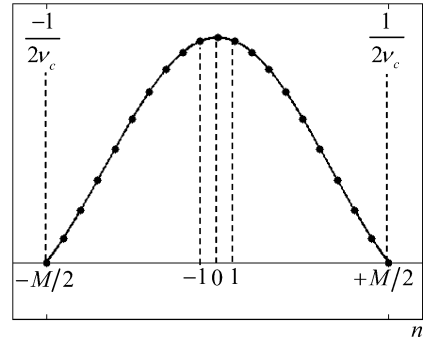


Fig. 4. Selection of the FIR coefficients.

M an even number. Note that causality is ensured in (16) because of the delay $M/2$

$$h_{FIR}(n) = h_{id}\left(n - \frac{M}{2}\right). \quad (16)$$

In order to avoid oscillations in the filtered response, we select coefficients from the h_{FIR} impulse response (16) that cover only the main lobe of the h_{id} “sinc” function (15), see Fig. 4. Thus, the filter order M becomes given by (17) where the “ceil” function returns the upper closest integer. By computing $h_{id}(n)$ (15) for $-M/2 < n < +M/2$, we obtain the coefficients of the FIR h_{FIR} (16)

$$M = 2 \text{ceil}\left(\frac{1}{2\nu_c}\right). \quad (17)$$

D. Filtering and Removal of Delay Effects

The application of the digital filter (16) to the ν th response data sequence $y^{(\nu)}(n)$ generates the output filtered response $y_f^{(\nu)}(n)$ by discrete convolution

$$y_f^{(\nu)}(n) = h_{FIR}(n) * y^{(\nu)}(n) = \sum_{m=0}^M h_{FIR}(m) y^{(\nu)}(n - m). \quad (18)$$

At the end, we eliminate *a posteriori* the delay introduced by the digital filter by removing the first $M/2$ samples of $y_f^{(\nu)}(n)$.

E. Cutoff Frequency and Implications for Initial Pole Specification

The normalized cutoff frequency ν_c is selected depending on the specific application. In general, usage of a small ν_c gives a reduced high-frequency content of the response, often allowing successful application of TD-VF with fewer poles. The tradeoff is reduced information at high frequencies.

The choice of ν_c has a direct impact on the specification of the initial poles $\{q_n\}$ of the TD-VF. These should be assumed linearly spaced in the interval (19), where T_w is the observation window length of the original time-domain samples

$$\left(\frac{1}{T_w}, \frac{1}{\Delta t} \nu_c\right). \quad (19)$$

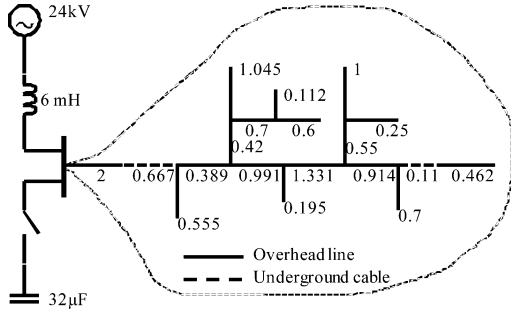


Fig. 5. Three-phase distributed system (distances in kilometers). The enclosed part is replaced with an FDNE.

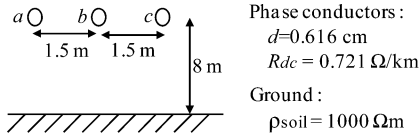


Fig. 6. Geometry of the overhead lines for the power system of Fig. 5.

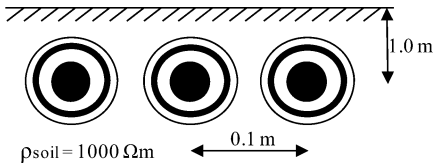


Fig. 7. Cable configuration for the power system of Fig. 5.

TABLE I
CABLE DATA

Item	Property
Core	$d=10.65$ mm, $\rho=4.179E-8$ Ω m
Insulation	$t=5.5$ mm, $\epsilon_r=2.3$
Sheath	$t=0.35$ mm, $\rho=1.724E-8$ Ω m
Jacket	$t=4$ mm, $\epsilon_r=2.3$

F. Windowing of the FIR Impulse Response

In practice, the first and last filter coefficients are not perfectly equal to zero, in particular, in cases with low filter orders. In these situations, one can still obtain zero start and end values by multiplying h_{FIR} with an appropriate window function (e.g., the Hanning window [23]).

V. EXAMPLE: MV DISTRIBUTION SYSTEM

A. FDNE Modeling

We consider the three-phase 24-kV rural distribution system described in [3], see Fig. 5. The system is composed of a set of overhead lines and underground cables. The electrical loads are ignored. Each line section consists of a flat untransposed overhead line without ground wires, while each cable section consists of three single core coaxial cables. All transmission lines and cables have the same geometry, see Figs. 6 and 7 and Table I. The objective is to calculate an FDNE model of the subnetwork indicated by the dashed line.

The behavior of the subnetwork is characterized in the time domain using the trapezoidal-based PSCAD circuit solver. A

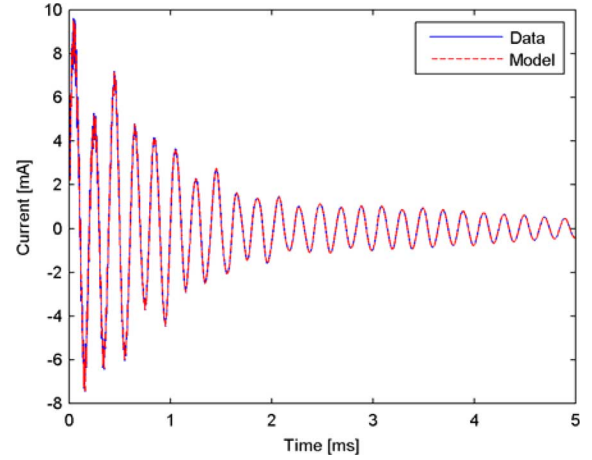


Fig. 8. Fitting model to data. Comparison between the original current response and the simulated model for the matrix element (1,1).

unit step voltage source is applied successively to the phases one by one with the other phases grounded. The applied voltages and the resulting current responses are recorded. We use a time step $\Delta t = 0.2 \mu\text{s}$ and a window length of 5 ms (25 000 samples). In order to reduce the required model order, the resulting matrix of current responses is postprocessed using the digital filter with normalized cutoff frequency $\nu_c = 0.04$. The resulting matrix of responses is stacked by its columns in an array of responses that is subjected to the multiport TD-VF algorithm described in Section III-C. (The symmetry permits us to use only the lower triangle of the matrix of current responses, thereby saving computation time.) We use a fitting order $N = 40$ and a relative adaptive sampling threshold $\delta = 1E-4$.

Fig. 8 compares element (1,1) of the input data with that of the filtered model response, demonstrating a highly accurate fitting result. A similar result is achieved for the other elements as well.

B. Simulation of the Capacitor Bank Energization

The FDNE is interfaced to PSCAD by the user-defined component in [12]. We now simulate the effect of energizing the capacitor bank in Fig. 5 when closing the circuit breaker simultaneously in all phases at $t = 0$. The simulation is run twice: 1) using the detailed circuit of Fig. 5 with all cables and overhead lines represented by frequency-dependent traveling-wave models and 2) with the subnetwork replaced by the FDNE model. In both simulations, a time step $\Delta t = 0.2 \mu\text{s}$ is used.

Figs. 9 and 10 (expanded view) show the current flowing through the phase a . It can be seen that both simulation approaches give about the same result. Similar results are achieved for the current in the other phases.

Use of the FDNE model reduces the CPU time of the simulation time from 71.6 to 13.6 s (i.e., giving a speed gain of 5.3), see Table II.

The FDNE is applicable with alternative time-step lengths provided that they are at least as long as the one used for the identification. Fig. 11 compares the simulated result for time-step lengths $2\Delta t$, $5\Delta t$, and $10\Delta t$, where Δt is the time step used for the FDNE model extraction. It can be seen that the simulated

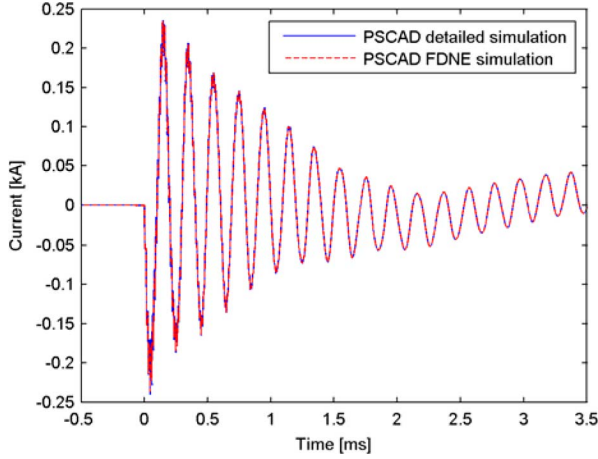


Fig. 9. Simulated current in phase a . A comparison between the PSCAD simulation result of the detailed network (Fig. 5) and the same network with FDNE.

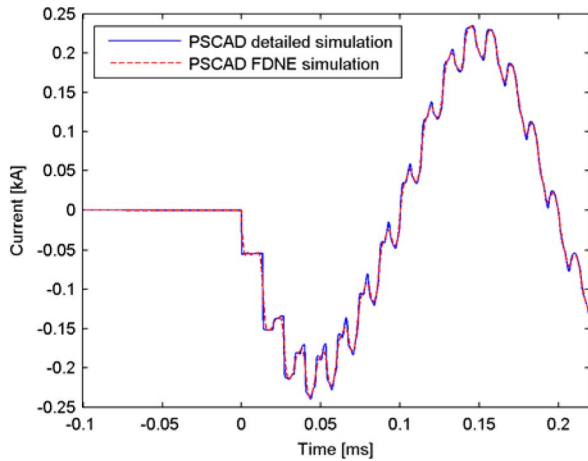


Fig. 10. Simulated current in phase a . Extended view of Fig. 9.

TABLE II
SIMULATIONS: CPU TIME RESULTS (IN SECONDS)

Detailed circuit	FDNE	Gain
71.6	13.6	5.3

result remains essentially unchanged, although the trapezoidal integration leads to some inevitable loss of accuracy.

C. Adaptive Sampling: CPU Time Results

We will now show the benefit of the adaptive sampling method in Section III-E that is used in the pole identification step. We use the same example as before but extend the time record from 5 to 10 ms (50 000 samples).

The dimension of each response block to be subjected to QR factorization (12) is $50\,000 \times 81$, with all samples considered. Table III shows the reduction in matrix rows (expressed by the number of kept rows) as a function of the threshold value used in the sampling process, and the resulting CPU time required by the subsequent QR factorization. In the previous sections, we used a $\delta = 1E - 4$, giving a 94% savings in CPU time.

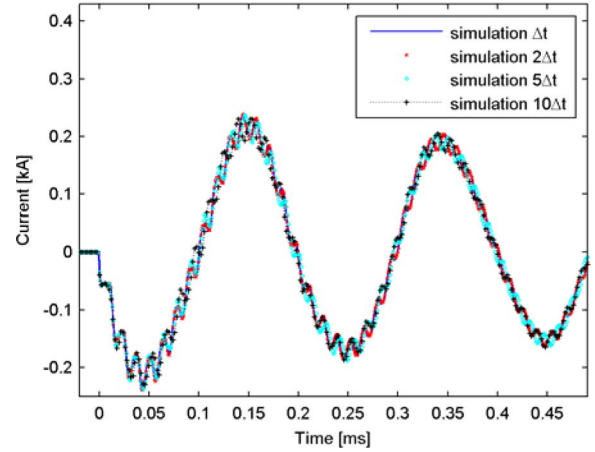


Fig. 11. Simulated current in phase a . Simulation for the network of Fig. 5 with the FDNE by using alternative time-step lengths.

TABLE III
TIMING QR FACTORIZATION (SINGLE RESPONSE BLOCK)

Adapt. sampling threshold, δ	N.o. rows kept [%]	CPU-time [milliseconds]
$1E-3$	4.01%	24.5
$1E-4$	12.1%	115
$1E-5$	27.6%	456
$1E-6$	54.3%	986
All samples	100%	1890

Adaptive sampling is applied only for the QR factorizations in the pole estimation step. In the residues computation step, we prefer using all samples since the computational cost is relatively small.

D. Numerical Filtering

In order to better appreciate the effect of the numerical filtering (Section IV), we modify the network in Fig. 5 by removing the 2-km overhead line between the bus and the cable. This greatly increases the front steepness of the current response. We repeat the generation of the starting data with the circuit solver using a time step $\Delta t = 0.1 \mu s$ and a window length of 3 ms (30 000 samples).

Two FDNE models are constructed: one using the original starting data and the other one using the filtered starting data with a low-pass filter having a normalized cutoff frequency $\nu_c = 0.05$. In the first case, we use a fitting order $N = 200$, whereas in the second case, we use $N = 140$.

Fig. 12 shows the simulated current flowing into phase b of the cable when energizing the capacitor bank at $t = 0$ ms. The result is shown for three different simulations of the current: simulation using the detailed network, using the FDNE model with the filter, and using the FDNE model without the filter. It can be seen that the filtering approach removes the spurious oscillations associated with the steep wavefronts of the response.

A further advantage of using the filter is that we can achieve models with a lower order, thereby reducing the complexity of the FDNE equivalent and, thus, the simulation time.

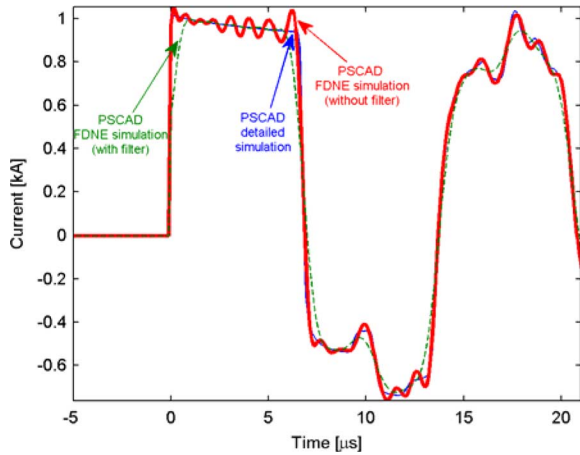


Fig. 12. Capacitor bank energization: simulated current in phase b .

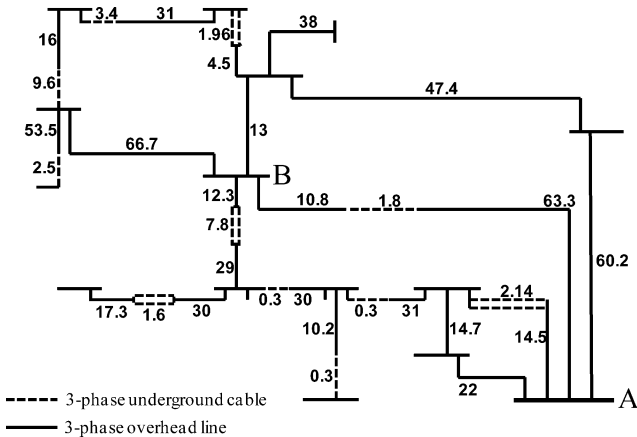


Fig. 13. Regional transmission network (distances in kilometers).

VI. EXAMPLE: REGIONAL TRANSMISSION SYSTEM

A. Power System

We now demonstrate the applicability of the FDNE modeling approach to a highly complex 145-kV regional transmission system (see Fig. 13). The objective is to calculate the FDNE equivalent of the entire network seen from bus A .

B. Computation of the FDNE

The system in Fig. 13 is modeled in PSCAD using a frequency-dependent traveling-wave model [24] for all lines and underground cables. The 3×3 matrix of current responses is obtained by applying step voltages to bus A with a time-step length $\Delta t = 0.2 \mu\text{s}$ and a window length of $T_w = 20$ ms. The obtained current responses (admittance) are processed using the low-pass filter with a normalized cutoff frequency $\nu_c = 0.005$. The resulting responses are subjected to TD-VF with a fitting order $N = 140$ and 20-pole relocating iterations, giving a common-pole model (3). In the pole identification step, the adaptive sampling approach is applied with a relative threshold $\delta = 1E - 4$. Finally, the model is subjected to passivity enforcement by residue perturbation [25].

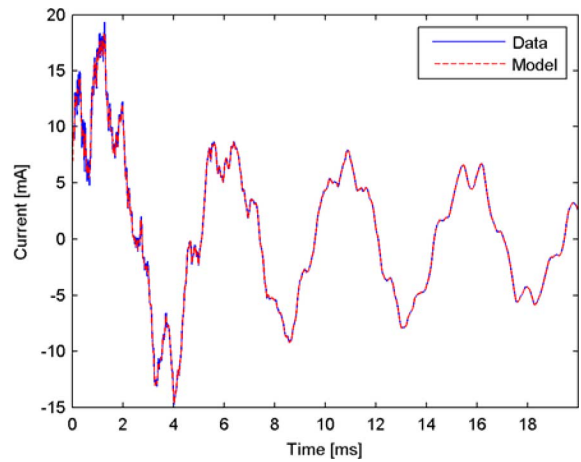


Fig. 14. Fitting model to data (with the filter approach). Comparison between the original current response and the simulated model for the matrix element (1,1).

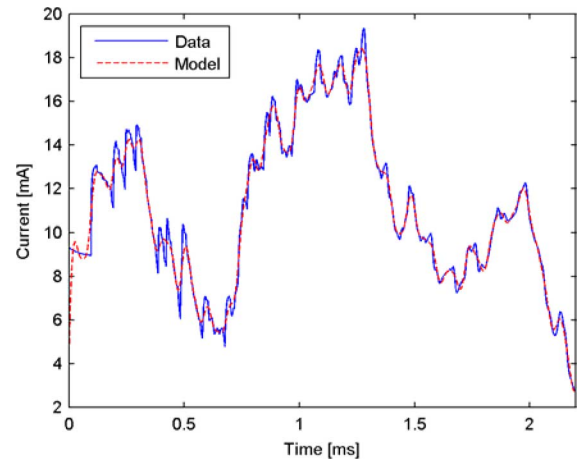


Fig. 15. Expanded view of Fig. 14.

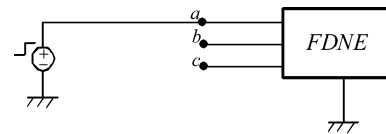


Fig. 16. Unit step voltage excitation.

The obtained model is quite accurate for all matrix elements. Fig. 14 shows the result for element (1,1). The expanded view in Fig. 15 shows the smoothing effect of the low-pass filter.

C. Voltage Simulation

Using the FDNE, we simulate the voltage response on phase b when applying a unit step voltage on phase a with phases b and c open (see Fig. 16).

Fig. 17 compares the voltage on phase b obtained by the FDNE with that of the detailed PSCAD model. It can be seen that a quite accurate result has been obtained.

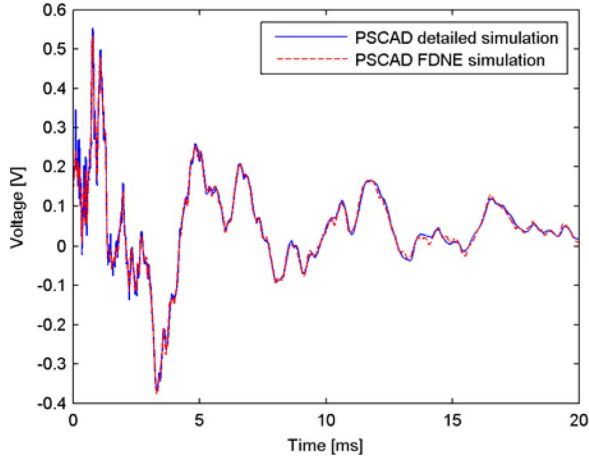


Fig. 17. Simulated voltage in phase b . Comparison between simulations using FDNE and the detailed PSCAD circuit.

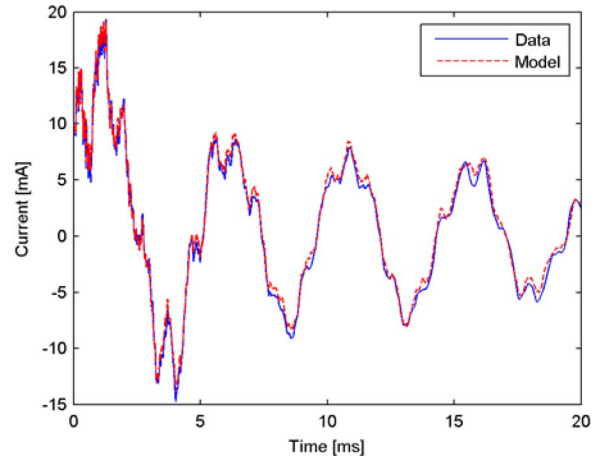


Fig. 19. Fitting model to data (without filter). Matrix element (1,1).

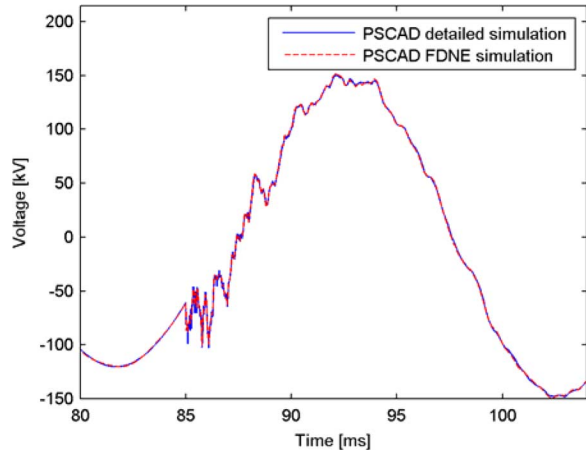


Fig. 18. Simulated voltage in phase b . Comparison between simulations using FDNE (plus current sources) and detailed PSCAD circuit.

TABLE IV
SIMULATIONS: CPU TIME RESULTS (IN SECONDS)

Detailed circuit	FDNE	Gain
38.3	5.11	7.5

D. Embedded Sources

We next demonstrate the handling of embedded sources. A 50-Hz three-phase 145-kV voltage source is connected to the internal bus B in Fig. 13. This source is handled by the procedure in Section II-D where the FDNE is modified and current sources are introduced. Fig. 18 shows a simulation result when the subsystem is operating in islanding mode. A ground fault occurs in phase a at voltage maximum ($t = 85$ ms). The plot compares the voltage on phase b obtained by the FDNE with that by the detailed PSCAD model. Clearly, a highly accurate result is achieved using the FDNE approach.

E. CPU Time Results

Similarly as in the previous example, usage of the FDNE approach leads to substantial savings in computation time when

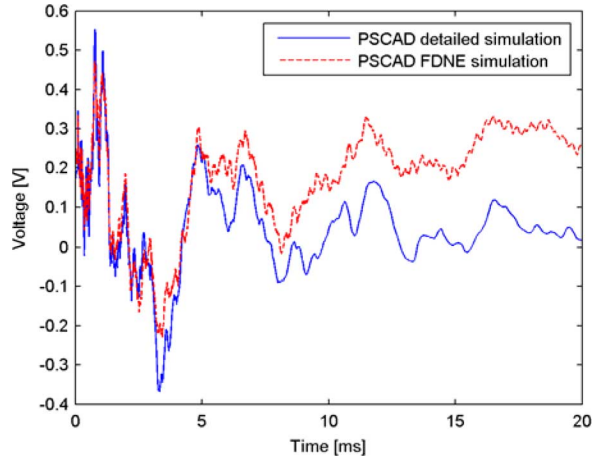


Fig. 20. Simulated voltage in phase b . Comparison between simulations using FDNE and detailed PSCAD circuit.

performing a transient simulation. Table IV shows a speed gain of 7.5 when conducting the voltage simulation in Section VI-C.

F. Results Without the Usage of the Filter

The usage of filtering not only avoids the occurrence of spurious oscillations; it is sometimes essential for obtaining a useful model.

Fig. 19 shows the result for element (1,1) of the matrix of current responses when the fitting is done without usage of the filtering. ($N = 250$ poles were used in the fitting process). It can be seen that accuracy is substantially lower compared to the result when using filtering, see Fig. 14. The accuracy did not substantially improve with alternative fitting orders.

The reduced accuracy can be detrimental in situations with high impedance terminations since error magnification effects can occur [22]. This is demonstrated in Fig. 20 when simulating the voltage response at phase b due to a step voltage excitation on phase a with phases b and c open. It can be seen that large errors develop with time. Therefore, the high accuracy achievable with the proposed TD-VF implementation is an essential feature.

VII. DISCUSSION

A. Time-Step Length

In the two examples of the paper, a time step of $\Delta t = 0.2 \mu s$ is used. This choice is based on the restriction that the time-step length with the detailed PSCAD model must be smaller than the smallest transmission-line traveling time (112-m overhead line in Example #1, 300-m cable in Example #2). Using a time step longer than the shortest travel time can lead to inaccurate results and even instabilities. This restriction does not exist with the FDNE model. It was shown in Section V-B that the time-step length could be increased from 0.2 to 2 μs with only a small change to the overall waveforms. Hence, large savings in computation time are possible compared to the detailed PSCAD simulation model.

B. Memory Requirements

In addition to savings in computation time, the FDNE approach can also lead to savings in memory requirements. For instance, in the second example, the total length of the overhead lines is 615.4 km. With an assumed propagation velocity of 300 m/ μs , the traveling-wave buffers (forward and backward waves) will with a time-step length of 0.2 μs contain about 20 500 cells per phase (i.e., a total of 61 500 cells). For comparison, the storage requirement is with the FDNE model dominated by the matrix of coefficients by which the state vector is multiplied [12]. With an order of $N = 140$ and $n = 3$ phases, this amounts to about $n^2 N = 1260$ cells. Thus, a reduction in storage by a factor of about 48 is achieved.

C. Handling of Unstable Poles in TD-VF

In this paper, the occurrence of unstable poles during the TD-VF iterations is handled by flipping any unstable pole into the left half plane, similar to the frequency-domain counterpart of VF [15]. However, we have observed with TD-VF that the pole flipping procedure may, in some rare cases, fail to produce an acceptable model. In those situations, an effective remedy is to disable the pole flipping. The computed model then has the restriction that it cannot be applied in simulations for a time T_{sim} longer than the one used in the fitting process T_w . This implies that the simulation cannot be initialized by ramping up the sources in a lengthy simulation ($T_{sim} > T_w$). The latter problem is not an issue with Electromagnetic Transients Program (EMTP) simulators that can initialize directly from a frequency-domain steady-state solution.

VIII. CONCLUSION

In this paper, we have presented an implementation of the TD-VF algorithm for the purpose of FDNE modeling of complex power systems from time-domain responses as follows.

- 1) The TD-VF algorithm is extended to multiport systems, giving a common-pole model based on poles and residue matrices.
- 2) A fast solution of the pole identification step is achieved by utilizing the special sparsity pattern of the system matrix.
- 3) An adaptive sampling approach is applied in order to reduce the number of rows in the system matrices during

pole identification. This greatly reduces the computation time for the FDNE model.

- 4) Filtering the time-domain input data before applying TD-VF is very useful, both reducing the required model order and avoiding spurious oscillations in the result; for that purpose, we apply a digital, FIR low-pass filter.
- 5) The extracted FDNE model is interfaced to PSCAD using recursive convolution. Application to a 24-kV distribution system and a 145-kV regional transmission system demonstrates the ability of the FDNE modeling approach to achieve highly accurate results.
- 6) The application of FDNE can give substantial reductions in simulation CPU times. For the two cases in this study, we obtained a speed gain by a factor of 5.3 and 7.5, respectively. Further savings can be achieved in situations where the subnetwork contains short lines as the FDNE can be applied with longer time-step lengths than the detailed model.
- 7) Usage of FDNE can lead to large savings in memory in situations where the subnetwork contains many transmission lines so that their total travel time is much larger than the simulation time-step length.

APPENDIX

A. Derivation of Multiport Formulation

Let us start with expression (A1), obtained by applying (7) to the ν th response evaluated for the sample at time $t = t_k$. The unknowns $\{\theta_n\}$ are common for all responses

$$y^{(\nu)}(t_k) = \sum_{n=1}^N m_n^{(\nu)} \tilde{u}_n^{(\nu)}(t_k) - \sum_{n=1}^N \theta_n \tilde{y}_n^{(\nu)}(t_k) + m_0^{(\nu)} u^{(\nu)}(t_k). \quad (A1)$$

Collecting all samples $[y^{(\nu)}(t_1) \dots y^{(\nu)}(t_K)]^T$ into the array $\mathbf{y}^{(\nu)}$, all unknowns $[m_0^{(\nu)} \dots m_N^{(\nu)}]^T$ and $[\theta_1 \dots \theta_N]^T$ into arrays $\mathbf{m}^{(\nu)}$ and $\boldsymbol{\theta}$, respectively, and finally defining matrices $\tilde{\mathbf{U}}^{(\nu)}$ and $\tilde{\mathbf{Y}}^{(\nu)}$

$$\tilde{\mathbf{U}}^{(\nu)} = \begin{pmatrix} \tilde{u}_1^{(\nu)}(t_1) & \dots & \tilde{u}_N^{(\nu)}(t_1) & u^{(\nu)}(t_1) \\ \vdots & & \vdots & \vdots \\ \tilde{u}_1^{(\nu)}(t_K) & \dots & \tilde{u}_N^{(\nu)}(t_K) & u^{(\nu)}(t_K) \end{pmatrix} \quad (A2)$$

$$\tilde{\mathbf{Y}}^{(\nu)} = \begin{pmatrix} \tilde{y}_1^{(\nu)}(t_1) & \dots & \tilde{y}_N^{(\nu)}(t_1) \\ \vdots & & \vdots \\ \tilde{y}_1^{(\nu)}(t_K) & \dots & \tilde{y}_N^{(\nu)}(t_K) \end{pmatrix} \quad (A3)$$

we achieve for $\mathbf{y}^{(\nu)}$, the following compact expression:

$$\mathbf{y}^{(\nu)} = \tilde{\mathbf{U}}^{(\nu)} \mathbf{m}^{(\nu)} + \tilde{\mathbf{Y}}^{(\nu)} \boldsymbol{\theta}. \quad (A4)$$

Finally, it is straightforward to obtain the linear system (10), writing (A4) for all responses $\nu = 1 \dots L$.

Here, we have considered, for the simplicity of notation, the same number of samples K for each response, but this procedure is applicable with an arbitrary number of samples.

REFERENCES

- [1] H. W. Dommel and W. S. Meyer, "Computation of electromagnetic transients," *Proc. IEEE*, vol. 62, no. 7, pp. 983–993, Jul. 1974.

- [2] A. Morched, J. Ottevangers, and L. Marti, "Multi-port frequency dependent network equivalents for the EMTP," *IEEE Trans. Power Del.*, vol. 8, no. 3, pp. 1402–1412, Jul. 1993.
- [3] B. Gustavsen, "Computer code for rational approximation of frequency dependent admittance matrices," *IEEE Trans. Power Del.*, vol. 17, no. 4, pp. 1093–1098, Oct. 2002.
- [4] M. Abdel-Rahman, A. Semlyen, and R. Iravani, "Two-layer network equivalent for electromagnetic transients," *IEEE Trans. Power Del.*, vol. 18, no. 4, pp. 1328–1335, Oct. 2003.
- [5] H. Singh and A. Abur, "Multi-port equivalencing of external systems for simulation of switching transients," *IEEE Trans. Power Syst.*, vol. 10, no. 1, pp. 374–382, Jan. 1995.
- [6] W. D. C. Boaventura, A. Semlyen, M. R. Iravani, and A. Lopes, "Sparse network equivalent based on time-domain fitting," *IEEE Trans. Power Del.*, vol. 17, no. 1, pp. 182–189, Jan. 2002.
- [7] T. Noda, "Identification of a multiphase network equivalent for electromagnetic transient calculations using partitioned frequency response," *IEEE Trans. Power Del.*, vol. 20, no. 2, pt. 1, pp. 1134–1142, Apr. 2005.
- [8] A. Ramirez, "Vector fitting-based calculation of frequency-dependent network equivalents by frequency partitioning and model-order reduction," *IEEE Trans. Power Del.*, vol. 24, no. 1, pp. 410–415, Jan. 2009.
- [9] M. Matar and R. Iravani, "A modified two-layer network equivalent for the analysis of electromagnetic transients," *IEEE Trans. Power Del.*, vol. 25, no. 1, pp. 434–441, Jan. 2010.
- [10] Y. Liang, X. Lin, A. M. Gole, and M. Yu, "Improved coherency-based wide-band equivalents for real-time digital simulators," *IEEE Trans. Power Del.*, vol. 26, no. 3, pp. 1410–1417, Aug. 2011.
- [11] A. Semlyen and A. Dabuleanu, "Fast and accurate switching transient calculations on transmission lines with ground return using recursive convolutions," *IEEE Trans. Power App. Syst.*, vol. PAS-94, no. 2, pp. 561–575, Mar./Apr. 1975.
- [12] B. Gustavsen and O. Mo, "Interfacing convolution based linear models to an electromagnetic transients program," in *Proc. Int. Conf. Power Syst. Transients*, Lyon, France, Jun. 4–7, 2007, p. 6.
- [13] E. C. Levy, "Complex curve fitting," *IRE Trans. Autom. Control*, vol. 4, pp. 37–44, May 1959.
- [14] C. K. Sanathanan and J. Koerner, "Transfer function synthesis as a ratio of two complex polynomials," *IEEE Trans. Autom. Control*, vol. AC-8, no. 1, pp. 56–58, Jan. 1963.
- [15] B. Gustavsen and A. Semlyen, "Rational approximation of frequency domain responses by vector fitting," *IEEE Trans. Power Del.*, vol. 14, no. 3, pp. 1052–1061, Jul. 1999.
- [16] B. Gustavsen and A. Semlyen, "Enforcing passivity for admittance matrices approximated by rational functions," *IEEE Trans. Power Syst.*, vol. 16, no. 1, pp. 97–104, Feb. 2001.
- [17] S. Grivet-Talocia and A. Ubolli, "A comparative study of passivity enforcement schemes for linear lumped macromodels," *IEEE Trans. Adv. Packag.*, vol. 31, no. 4, pp. 673–683, Nov. 2008.
- [18] A. Ubolli and B. Gustavsen, "Comparison of methods for rational approximation of simulated time domain responses: ARMA, ZD-VF and TD-VF," *IEEE Trans. Power Del.*, vol. 26, no. 1, pp. 279–288, Jan. 2011.
- [19] S. Grivet-Talocia, "Package macromodeling via time-domain vector fitting," *IEEE Trans. Microw. Wireless Compon. Lett.*, vol. 13, no. 11, pp. 472–474, Nov. 2003.
- [20] D. Traina, G. Macchiarella, and T. K. Sarkar, "Robust formulations of the Cauchy method for microwave duplexers modeling," *IEEE Trans. Microw. Theory Tech.*, vol. 55, no. 5, pp. 974–982, May 2007.
- [21] D. Deschrijver, M. Mrozowski, T. Dhaene, and D. De Zutter, "Macro-modeling of multiport systems using a fast implementation of the vector fitting method," *IEEE Microw. Wireless Compon. Lett.*, vol. 18, no. 6, pp. 383–385, Jun. 2008.
- [22] B. Gustavsen and C. Heitz, "Fast realization of the modal vector fitting method for rational modeling with accurate representation of small eigenvalues," *IEEE Trans. Power Del.*, vol. 24, no. 3, pp. 1396–1405, Jul. 2009.
- [23] B. Boulet, *Fundamentals of Signals & Systems*, 1st ed. Hingham, MA: Da Vinci Engineering Press, Charles River Media, 2006.
- [24] A. Morched, B. Gustavsen, and M. Tartibi, "A universal model for accurate calculation of electromagnetic transients on overhead lines and underground cables," *IEEE Trans. Power Del.*, vol. 14, no. 3, pp. 1032–1038, Jul. 1999.
- [25] B. Gustavsen, "Fast passivity enforcement for pole-residue models by perturbation of residue matrix eigenvalues," *IEEE Trans. Power Del.*, vol. 23, no. 4, pp. 2278–2285, Oct. 2008.

Andrea Ubolli (M'10) received the Laurea and Ph.D. degrees in electronic engineering from Politecnico di Torino, Torino, Italy, in 2003 and 2008, respectively.

In 2004, he joined the EMC Group, Department of Electronics, Politecnico di Torino, as a Research Assistant, working on interconnect macromodeling and helping in the development of the IdEM tool. From 2005 to 2008, he was pursuing the Ph.D. degree, working on robust passive macromodeling of signal and power distribution networks in high-speed electronic systems. Since 2009, he has been a Postdoctoral Researcher with SINTEF Energy Research in cooperation with the University of Trondheim (NTNU), Trondheim, Norway, where he is working on frequency-dependent modeling of power systems.

Dr. Ubolli was the recipient of a Lagrange Project scholarship, supporting his research on complex systems modeling.

Bjørn Gustavsen (M'94–SM'03) was born in Norway in 1965. He received the M.Sc. and Dr.Eng. degrees from the Norwegian Institute of Technology (NTH), Trondheim, Norway, in 1989 and 1993, respectively.

Since 1994, he has been working at SINTEF Energy Research, where he is currently a Senior Research Scientist. His interests include the simulation of electromagnetic transients and modeling of frequency-dependent effects. He spent 1996 as a Visiting Researcher at the University of Toronto, Toronto, ON, Canada, and the Manitoba HVDC Research Centre, Winnipeg, MB, Canada, in 1998.

Dr. Gustavsen was a Marie Curie Fellow at the University of Stuttgart, Stuttgart, Germany, from 2001 to 2002.